



Power Electronic Systems
Laboratory

© 2011 IEEE

Proceedings of the 37th Annual Conference of the IEEE Industrial Electronics Society (IECON 2011), Melbourne, Australia, November 7-10, 2011.

Electronically Controllable Impedance for Tuning of Active Metamaterials

D. O. Boillat
T. Friedli
J.W. Kolar

This material is posted here with permission of the IEEE. Such permission of the IEEE does not in any way imply IEEE endorsement of any of ETH Zurich's products or services. Internal or personal use of this material is permitted. However, permission to reprint/republish this material for advertising or promotional purposes or for creating new collective works for resale or redistribution must be obtained from the IEEE by writing to pubs-permissions@ieee.org. By choosing to view this document, you agree to all provisions of the copyright laws protecting it.



Eidgenössische Technische Hochschule Zürich
Swiss Federal Institute of Technology Zurich

Electronically Controllable Impedance for Tuning of Active Metamaterials

David O. Boillat, Thomas Friedli, and Johann W. Kolar
Power Electronic Systems Laboratory, ETH Zurich, Switzerland
boillat@lem.ee.ethz.ch, www.pes.ee.ethz.ch

Abstract—Increasing population density and the consequential increased demand of electrical energy require the integration of electrical infrastructure for power distribution into residential areas and buildings. In order to meet the installation standards regarding the critical value of field emissions, the magnetic stray field of the electric equipment needs to be shielded. One shielding option is to realise an active shield in the form of a metamaterial, (a concept known from high-frequency engineering). A metamaterial is in this case composed by an array of base units, each one containing a *LCR*-resonator and a control unit called Electronically Controllable Impedance (ECI). The ECI consists of a 4-quadrant power converter with integrated measurement and control units for emulating an arbitrary impedance. The ECIs are used to tune the *LCR* resonators such that the metamaterial exhibits a paramagnetic or diamagnetic behaviour when excited by an external field. Thereby, each single *LCR*-resonator's resonant frequency is adjusted to the excitation frequency and the resonator's quality factor *Q* is optimally selected. This paper shows different realisations of an ECI and proposes an ECI control algorithm to tune the resonant frequency and to adjust the quality factor *Q* of the resonators. Furthermore, an experimental verification of the ECI concept is provided.

I. INTRODUCTION

Along with a continuing increase of population density and/or demand of electrical energy, electrical installations for power distribution are progressively integrated into residential areas and buildings. Since these power installations generate magnetic stray fields and the magnetic field strength is limited by standards, a shielding is often required in order to comply with the norms.

For example, in the year 2000, the new standard “Protection from Non-Ionising Radiation” (NISV) became effective in Switzerland to avoid harmful or disagreeable influences to the human body of magnetic stray fields generated by electrical power installations [3]. The installation rms *B*-field limit for a transformer substation is for instance fixed to $B_c = 1 \mu\text{T}$ at nominal power. As it can be exemplarily seen from Fig. 1, the stray field of a transformer is only

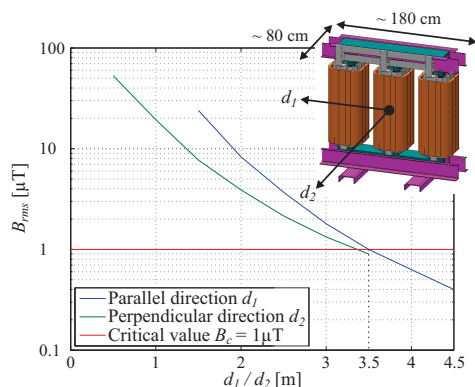


Fig. 1 Measured magnetic stray field (rms-values) for a 1 MVA/10 kV (50 Hz) dry-type distribution transformer from ABB (Resibloc) [1], [2].

below this critical value B_c at a distance of 3.5 m from the centre. As this is valid for the parallel as well as the perpendicular directions d_1 and d_2 , respectively, an area of $A_n = 7 \text{ m} \cdot 7 \text{ m} = 49 \text{ m}^2$ could not be utilised (for an installation in free space) in order to fulfil the standard. The base area of the transformer is approximately 1.44 m^2 and thus only 3% of A_n . This example demonstrates that shielding of the magnetic field of electrical power installations is necessary if the area A_n and the associated infrastructure costs should be reduced.

The described issue is exemplarily explained for Switzerland. However, other countries undergo the same trend. In relation with the magnetic field shielding of transformers, the shielding of the outgoing bus bar of the transformer is also important, as under certain conditions the magnetic stray field of the bus bar is dominant in the far field range [4].

Magnetic field shielding can be done passively with ferromagnetic materials or actively by generation of a compensating field. The compensating field can be generated by electrically conducting structures carrying controlled currents. At high frequencies ($> 1 \text{ MHz}$), the interaction of electromagnetic waves with a material may be modelled by *LCR*-resonators [5], [6]. The resonators are conducting currents and thus interacting with neighbouring resonators. Therefore, such resonators are able to generate a magnetic field which could compensate and/or shield another magnetic field. Accordingly, active shielding can be implemented following the same principle. The explained modelling technique is well established for metamaterials and antennas at high frequencies ($> 1 \text{ MHz}$), but could theoretically also be applied at low- and medium-frequencies (e.g. 50 Hz ... 50 kHz) to reach active shielding. A possible visualisation of the basic idea is given in Fig. 2 and explained based on the structure of metamaterials.

In this paper, as in [5]–[7], a metamaterial is in general understood as an artificial material or arrangement of structures with electromagnetic properties which is not commonly found in nature or which exhibits stronger electromagnetic effects than a natural one.

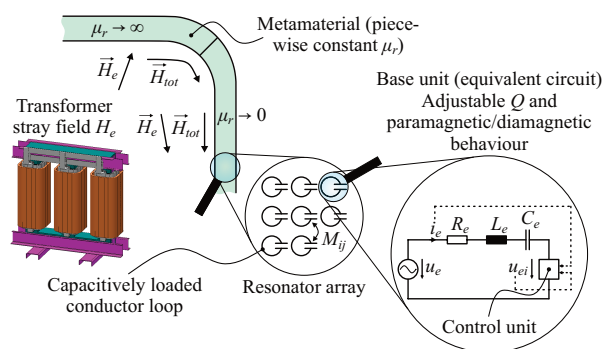


Fig. 2 Possible idea of shielding magnetic field with a metamaterial (transformer picture taken from [1]).

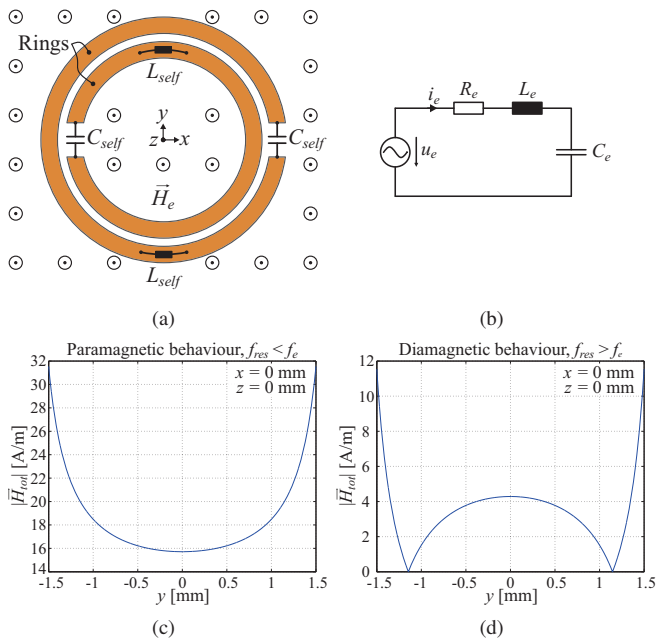


Fig. 3 Split ring resonator in an external field \vec{H}_e (a), LCR -resonator equivalent circuit with the induced voltage u_e as excitation (b) and qualitative plot of the total magnetic field magnitude $|\vec{H}_{tot}| = |\vec{H}_e + \vec{H}_i|$ inside the SRR for a paramagnetic (c) and diamagnetic (d) behaviour ($|\vec{H}_e| = 10 \text{ A/m}$).

Examples are a negative real part of the resulting permittivity [8] and/or permeability [9], [10], a negative [10] or an unusual high [11] real part of the refraction index in a certain frequency range. The word “resulting” is used in the sense that for an incident electromagnetic wave, the metamaterial acts like a compact material having the same uniform permittivity and permeability as the resulting ones. The parameters can be regarded as “resulting” if the wavelength of an incident wave is much larger than the dimensions of the material. In general, the permittivity $\underline{\epsilon} = \epsilon' + j\epsilon''$ and the permeability $\underline{\mu} = \mu' + j\mu''$ are complex quantities. The real parts correspond to $\epsilon' = \epsilon_r \epsilon_0$ and $\mu' = \mu_r \mu_0$, respectively. The imaginary parts ϵ'' and μ'' are related to the polarisation losses and the magnetic losses in the material, respectively [12]. The real part of the resulting permeability μ' is of primary interest for shielding magnetic fields with a metamaterial.

To reach a required field-strength reduction with the metamaterial, the magnetic field distribution in space should be changed in a desired manner. This can be achieved by emulating a constant permeability of the material in a given area (Fig. 2). This could be obtained by assembling a certain number of base units in an array as depicted in Fig. 2. One base unit consists of a resonator and an adequate control unit (Fig. 2). This is explained in the following.

In [10], a time varying homogeneous magnetic field \vec{H}_e with a frequency f_e is applied parallel to the z -axis of a Split Ring Resonator (SRR) as shown in Fig. 3(a). The magnetic field induces voltages which drive currents in the two rings of the SRR. Depending on whether the self-resonant frequency f_{self} of the SRR is below or above the excitation frequency f_e , the currents generate a magnetic field \vec{H}_i which enforces or weakens the external magnetic field \vec{H}_e . Thus, in the case where the magnetic field is increased inside the rings ($f_{self} < f_e$), the SRR acts as a paramagnet [$\mu_r > 1$, cf. Fig. 3(c)]. In

the opposite case ($f_{self} > f_e$), where the field is decreased inside the rings, the SRR behaves as a diamagnet [$0 \leq \mu_r < 1$, cf. Fig. 3(d)]. The resonance properties are built by the distributed (self-) inductance and capacitance of the SRR. Instead of the SRR, other resonators such as a capacitively loaded conductor loop can be employed to form the metamaterial [13]. The equivalent circuit of a LCR -resonator is depicted in Fig. 3(b). u_e is the voltage induced by the magnetic field \vec{H}_e and the capacitor C_e is implemented using foil capacitors. Furthermore, L_e is the inductor of a conductor loop used to generate the compensating field, but which is implemented by a discrete inductor in this paper in order to reach a compact test setup. For the same reason, an excitation frequency of $f_e = 1 \text{ kHz}$ instead of 50 Hz was selected.

By arranging such loops in close proximity to generate a periodic structure (Fig. 2), a strong magnetic coupling between the resonators occurs at a frequency close to the self-resonant frequency of a single resonator. The coupling strength increases the higher the quality factor Q of each single resonator is and the closer the frequency f_e is to the self-resonant frequency of the resonator. This coupling allows the entire metamaterial to show unique resulting permeability properties [10].

In summary, one resonator should emulate a paramagnetic or diamagnetic behaviour, and its quality factor Q , at the frequency f_e , should be controlled in order to adjust the coupling strength between the resonators. The interaction between the different resonators can be modelled with mutual inductances M_{ij} . In consequence, the quality factor Q of a single resonator is influenced by the other resonators in its proximity. Furthermore, the discrete elements may have tolerances, vary with temperature, or do not allow a desired quality factor to be reached without complicated constructions. Despite these influences and limitations, a single resonator should be kept at a certain quality factor Q for emulating a desired paramagnetic or a diamagnetic behaviour.

To bring the described idea to practice, several issues besides the realisation of the base unit need to be clarified, as e.g. the control of the different base units, the selection of the field sensors, the geometry of the magnetic field generating structure and the energy efficiency as well as costs of the entire system. This paper focuses only on the realisation, control and implementation of the base unit depicted in Fig. 2. As shown in the figure, a control unit is added to the circuit of Fig. 3(b) for adjusting the paramagnetic (capacitive) or diamagnetic (inductive) behaviour as well as controlling the quality factor Q at the frequency f_e to a desired value. The control unit is subsequently referred to as Electronically Controllable Impedance (ECI) and is described in **Section II**. In **Section III**, a possible control algorithm, which is implemented on the ECI, is introduced and analysed by simulations. The hardware prototype and measurements are shown in **Section IV**. The paper concludes with **Section V**, in which further fields of application for an ECI are described.

II. ELECTRONICALLY CONTROLLABLE IMPEDANCE

The conceptual idea of an Electronically Controllable Impedance is to electronically emulate an impedance in all four quadrants of the complex impedance plane. Four quadrant operation is required, as it may be possible that the ECI needs to deliver or absorb active and reactive power. This can be achieved by a Voltage Controlled Current Source (VCCS) or a Current Controlled Voltage Source (CCVS) with adequate control and measurement devices for delivery and absorption of active as well as reactive power. In the case of a

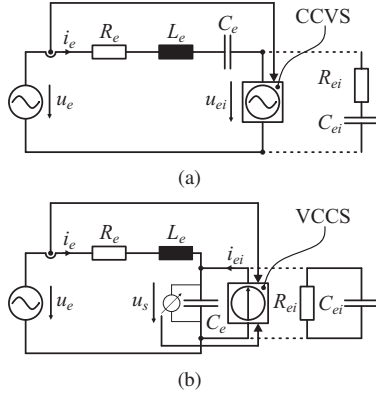


Fig. 4 Electronically tuned series (a) and parallel (b) resonant circuit.

CCVS, if the emulated impedance is $\underline{Z}_{ei} := z_{ei} \cdot e^{j\Delta\phi_{ei}}$, the voltage at the output of the source results in

$$u_{ei}(t) = \hat{i}_e \cdot z_{ei} \cdot \sin(\omega_e t + \Delta\phi_{ei}), \quad (1)$$

where \hat{i}_e is the amplitude and $\omega_e t + \phi_{ie}$ denotes the phase of the current i_e with respect to a reference frame. In (1), as below, it is assumed that the excitation is sinusoidal with only one frequency component at f_e .

There are two main possibilities of combining the ECI with the LCR -resonant circuit of Fig. 3(b), which are depicted in Fig. 4. Seen from the controlled source, a series resonant circuit is shown in Fig. 4(a) and a parallel resonant circuit in Fig. 4(b). It is assumed that the impedance of the circuit in Fig. 3(b) is given at a certain angular frequency ω by

$$\underline{Z}_e(\omega) = R_e + j\omega L_e + \frac{1}{j\omega C_e}. \quad (2)$$

R_e is in relation to the damping factor $\delta = \frac{1}{2} \frac{R_e}{L_e}$ of the circuit [Fig. 3(b)], while L_e as well as C_e determine the self-resonant frequency ($f_{self} = \frac{1}{2\pi\sqrt{L_e \cdot C_e}}$) of the same circuit. The quality factor Q at a certain angular frequency ω is related to the damping factor δ over

$$Q := \frac{\omega}{2\delta}. \quad (3)$$

In order to obtain, ideally, an infinitely high quality factor Q at a given frequency f_e , it is required that

- 1) the damping factor δ of the resonant circuit should be decreased (ideally to zero), and
- 2) the resonant frequency f_{res} of the resulting circuit (Fig. 4) should be tuned to the excitation frequency.

By adding an ECI \underline{Z}_{ei} [as for instance schematically depicted in Fig. 4(a)] to the circuit, the total impedance $\underline{Z}_{tot} = \underline{Z}_e + \underline{Z}_{ei}$ can be varied in such a way that the two requirements can be fulfilled as briefly demonstrated below. A possible circuit model of the ECI consists of series $C_{ei}R_{ei}$ -branch as shown in Fig. 4(a). In this case, the damping factor δ_0 and the resonant angular frequency ω_{res} are given to

$$\delta_0 = \frac{1}{2} \frac{R_e + R_{ei}}{L_e}, \quad (4)$$

$$\omega_{res} = \sqrt{\omega_{res,t}^2 - \delta_0^2} = \sqrt{\frac{1}{C_e^2 L_e^2} - \frac{1}{4} \frac{(R_e + R_{ei})^2}{L_e^2}}, \quad (5)$$

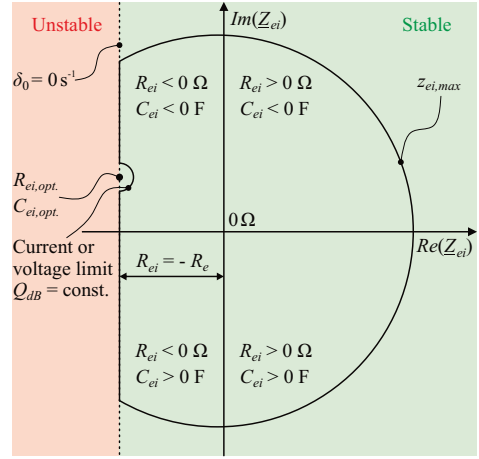


Fig. 5 Typical operating area in the complex impedance plane of an Electronically Controllable Impedance \underline{Z}_{ei} .

where $C_t = \frac{C_e C_{ei}}{C_e + C_{ei}}$. For $Q \rightarrow \infty$, the resistance R_{ei} and the capacitance C_{ei} result in

$$R_{ei,opt.} = -R_e, \quad (6)$$

$$C_{ei,opt.} = \frac{C_e}{\omega_e^2 L_e C_e - 1}. \quad (7)$$

It can be seen from the equation above that the resistance R_{ei} is negative in order to compensate the resistance R_e inherently present in the circuit. The system's damping is accordingly reduced by R_{ei} , which allows the first requirement to be fulfilled. C_{ei} enables to shift the resonant frequency of the entire circuit to the one of the excitation. Thus, the second requirement can be satisfied. In summary, considering Fig. 4(a), the real part of the impedance \underline{Z}_{ei} is related to the damping and the imaginary part of it to the tuning of the resonant frequency.

A typical plot of allowable impedance values of \underline{Z}_{ei} in the complex plane is given in Fig. 5. If the real part of the impedance is smaller than $-R_e$, the circuit is unstable, as the damping factor is negative. The signs of the resistance R_{ei} and capacitance C_{ei} are indicated in the figure for all four quadrants. The borderlines are given by the maximal admissible magnitude of the impedance \underline{Z}_{ei} , by the stability limit and by the maximal allowable voltage or current amplitude, $\hat{u}_{ei,max}$ and $\hat{i}_{e,max}$. The voltage or current limit applies first, depending on the desired operating point of the resonant circuit. The maximal impedance magnitude $z_{ei,max}$ is not a strong criteria, as for large values of z_{ei} the voltage amplitude \hat{u}_{ei} converges to the one of the excitation \hat{u}_e .

Due to the ECI's ability to tune the entire impedance of the series resonant circuit, the circuit of Fig. 4(a) is named Electronically Tuned Series Resonant Circuit (ETSRC) subsequent. Similar thoughts apply to the circuit of Fig. 4(b). Correspondingly, the circuit is called Electronically Tuned Parallel Resonant Circuit (ETPRC). The following considerations are focused on the ETSRC, as the paper's purpose is to demonstrate the concept.

III. ECI CONTROL ALGORITHM AND SIMULATIONS

Variations in the excitation frequency f_e can lead to changes in the values of the capacitance C_e and inductance L_e . In addition, the resistance R_e and the parasitic resistances of C_e and L_e or

the mentioned components themselves may vary with temperature. Furthermore, tolerances in the values of the components may make it difficult to reach the desired Q -factor. To overcome these limitations, this section presents a control algorithm which is able to obtain and keep a certain quality factor Q , despite varying parameters. Changes in the component values resulting from temperature variations occur within the order of seconds. Thus, the control algorithm needs to be “fast enough” to follow these component variations. Alteration of the excitation frequency could occur during electrical dynamic transients in the device to shield, but are not considered as prevalent.

The quality factor Q_{dB} is in this paper defined as

$$Q_{dB} := 20 \cdot \log_{10} \left(\frac{\hat{i}_e}{\hat{u}_e} \right). \quad (8)$$

The unit of Q_{dB} is dBS (decibel siemens). There are two main reasons for introducing this new definition. Firstly, a direct relation between the quality factor Q_{dB} and the current, which is the magnetic field constituent quantity, is obtained. Secondly, the damping factor in (3) can be dependent on the capacitance C_{ei} as well as on the resistance R_{ei} . This is not the case for the ETSRC but for the ETPRC [Z_{ei} can be modelled with a parallel $C_{ei}R_{ei}$ -branch, cf. Fig. 4(b)]. Variations of C_{ei} and R_{ei} may lead to very low damped eigenmodi at different frequencies than f_e . Nevertheless, these eigenmodi show “high” conventional quality factors Q (Eq. 3) (even though the current amplitude \hat{i}_e is “low”), which makes a clear illustration difficult.

The calculated steady-state quality factor Q_{dB} is plotted in Fig. 6 as a function of the ECI $Z_{ei} = z_{ei} \cdot e^{j\Delta\phi_{ei}}$ for the parameters given in Table I. The lines with the same quality factor are called equiquality-lines. In addition to the equiquality-lines, the phase of the impedance Z_{tot} is also depicted in the figure. It can be seen from Fig. 6 that the maximum quality factor $Q_{dB,max}$ is limited by the maximum current or voltage amplitude, for which the ECI is designed. However, along the line with $Q_{dB,max}$, different phases ϕ_{tot} of the total impedance Z_{tot} are obtained. Both, $\phi_{tot} = -90^\circ$ and $\phi_{tot} = 90^\circ$ can be reached. In the former case, the ETSRC acts like a capacitor (u_e lags i_e) and in the latter one like an inductor (i_e lags u_e). As the phase-shift between the external magnetic field and the induced voltage is -90° (Faraday’s law of induction), a capacitive behaviour results in paramagnetic and an inductive one

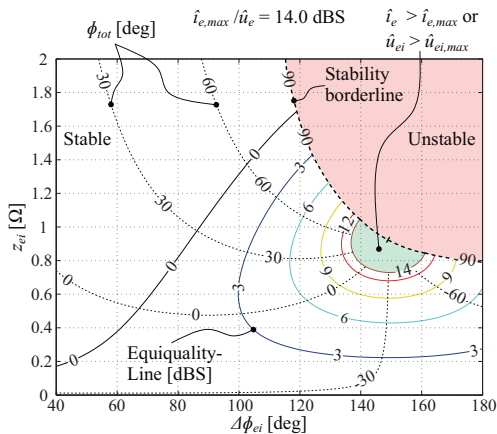


Fig. 6 Steady-state quality factor Q_{dB} plotted over the phase $\Delta\phi_{ei}$ and the magnitude z_{ei} of the ECI Z_{ei} (the phase ϕ_{tot} of $Z_{tot} = Z_e + Z_{ei}$ is also given in the plot).

in diamagnetic properties of the ETSRC. Thus, in addition to adjust Q_{dB} of one single resonator, the circuit can evoke a paramagnetic or diamagnetic behaviour when exposed to the external magnetic field \vec{H}_e .

The closer an operating point lays to the stability border (dashed line in Fig. 6) the less changes in the impedance Z_{ei} are damped and consequently the longer it takes to reach a quasi-steady state. Thus, an operation at the stability border is not reasonable. This means that a certain stability margin needs to be considered, which rejects a pure capacitive/inductive behaviour of the ETSRC. Therefore, a paramagnetic/diamagnetic behaviour is subsequently understood as a predominately paramagnetic/diamagnetic operating point.

A flow chart of the control algorithm is shown in Fig. 7. The

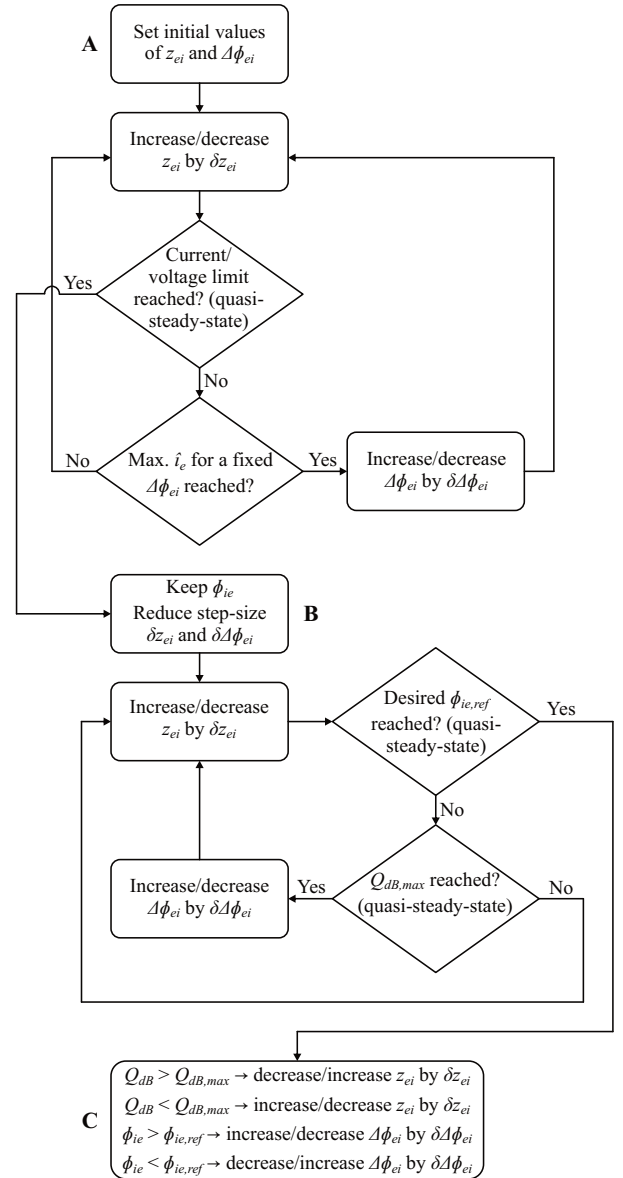


Fig. 7 Flow chart of the control algorithm implemented on the ECI (for $f_e < f_{self}$, $\Delta\phi_{ei}$ is increased while for $f_e > f_{self}$ it is decreased; starting point for the control algorithm’s path in Fig. 8 is $z_{ei} = 0.1 \Omega$ and $\Delta\phi_{ei} = 100^\circ$; A, B, C refer to Fig. 8 and Fig. 11).

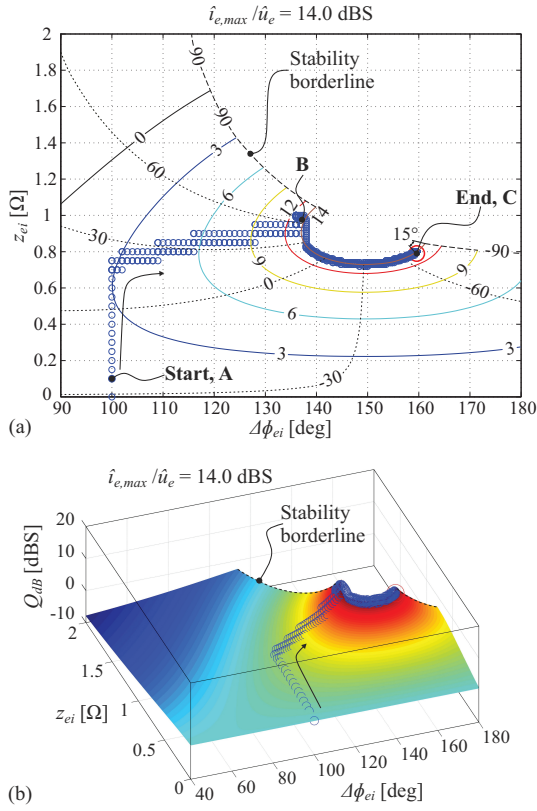


Fig. 8 2D (a) and 3D (b) plot of the control algorithm's path (blue circles) in the $\Delta\phi_{ei}$ - z_{ei} -plane (emulated capacitive (paramagnetic) behaviour).

voltage $u_{ei}(t)$ is applied to the resonant circuit as given by (1). Therefore, one task could be the maximisation of the quality factor Q_{dB} . This comprises to find the magnitude z_{ei} and the phase $\Delta\phi_{ei}$ in such a way that the current amplitude \hat{i}_e [Eq. (8)] is maximised (along with the indicated limitations). Firstly, an appropriate starting point is selected based on the measured circuit parameters (A). A point consists of two values, z_{ei} and $\Delta\phi_{ei}$. Then, the magnitude z_{ei} , which leads to the highest possible Q_{dB} -factor for a fixed $\Delta\phi_{ei}$, is adjusted (in discrete steps δz_{ei}) by measuring the current amplitude \hat{i}_e and comparing it with previous values. If this point is found, the phase $\Delta\phi_{ei}$ is increased in the right direction by one step $\delta\Delta\phi_{ei}$ and the magnitude z_{ei} is again selected such that the highest Q_{dB} results. This sequence is repeated until the previously mentioned current or voltage limit is reached (B). In a next step, the capacitive or inductive behaviour of the ETSRC is adjusted. As the damping can be further reduced by this adjustment, it is meaningful to decrease the step sizes δz_{ei} and $\delta\Delta\phi_{ei}$. When the current or voltage limit is reached, the phase ϕ_{ie} of the current i_e (with respect to a reference frame) is locked. This allows the phase to be shifted by the required amount (ϕ_{ie} is an effigy of ϕ_{tot}). The tuning of the ECI Z_{ei} in this loop is done in the same way as described above. Once the current-phase ϕ_{ie} has reached the desired value $\phi_{ie,ref}$, the algorithm remains in the attained operating point (C). However, it still keeps controlling the magnitude z_{ei} and phase $\Delta\phi_{ei}$ in the described manner. It should be noted that the presented control algorithm is one of many options. In addition, instead of measuring the phase ϕ_{ie} of the current i_e and shifting the phase of the voltage u_{ei} by $\Delta\phi_{ei}$, it would be possible

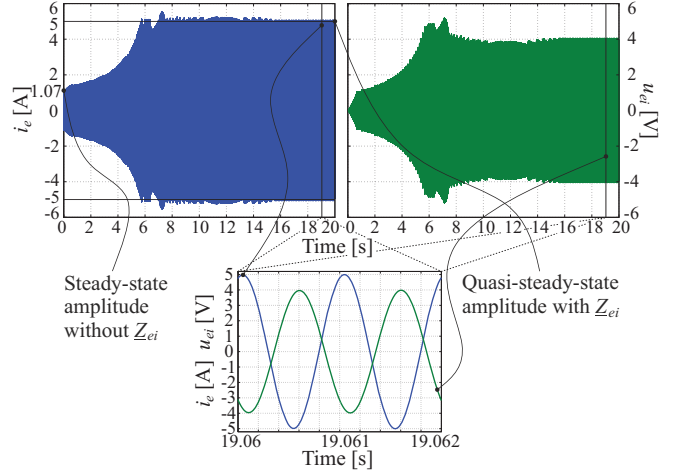


Fig. 9 Time behaviour of the resonator current $i_e(t)$ (blue) and the ECI voltage $u_{ei}(t)$ (green) for an emulated capacitive (paramagnetic) behaviour.

to replace $\Delta\phi_{ei}$ by a delay $T_{d,ei}$, by which the voltage $u_{ei}(t)$ is retarded with respect to the current $i_e(t)$. This may be advantageous if $u_e(t)$ is not purely sinusoidal.

The simulation parameters are summarised in Table I. The current amplitude \hat{i}_e , for the given circuit parameters, is bounded by the maximum current $\hat{i}_{e,max}$. In order not to operate the system at the limit of stability, the maximal amplitude of the current i_e is fixed to 5 A. The path of the control algorithm for an emulated capacitive (paramagnetic) behaviour in the $\Delta\phi_{ei}$ - z_{ei} -plane is plotted in Fig. 8 (blue circles). The end point is given with a larger (red) circle. The phase margin to the unstable area is 15° . The time behaviour of the current $i_e(t)$ and the voltage $u_{ei}(t)$ for this case are depicted in Fig. 9. The path in the case of an emulated inductive (diamagnetic) behaviour would be similar to the one depicted in Fig. 8 and is hence not shown. The simulations were run in MATLAB/Simulink. As demonstrated by the example, a nearly five times higher current amplitude \hat{i}_e can be reached by actively controlling the resonator with an ECI. In this way, a quality factor of $Q_{dB,t} = 14.0$ dBs is reached (at 1 kHz). Without the electronic impedance, $Q_{dB,nt} = 0.6$ dBs is obtained, which is a factor 22.2 lower. Furthermore, by the same means, the resonant frequency of the resonant circuit could be moved from 1.1 kHz to 1 kHz. Frequency shifts in the other direction and by other amounts are possible as well. The control algorithm introduced in this paper is fast enough (update rate of 25 ms) to compensate temperature dependent changes of the resistance, which lies in the order of seconds. Also, it can be seen from (1) that with the algorithm shown, the circuit can be adapted to changes in the excitation frequency, as $\phi_{ie} = \omega_e t$ is directly employed to form the voltage $u_{ei}(t)$.

IV. ECI PROTOTYPE AND MEASUREMENTS

The ECI hardware prototype shown in Fig. 10 was built to experimentally verify the suggested ECI concept and control algorithm. The power operational amplifier OPA549 from TI/Burr-Brown was selected as controlled voltage source. The control logic is implemented on a TI TMS320F2808 DSP and a Lattice FPGA. The control code is executed at 100 kHz. For testing purpose, the excitation voltage $u_e(t)$ is generated by a linear 4-quadrant amplifier PAS1000 from Spitzenberger&Spies instead of being induced by an

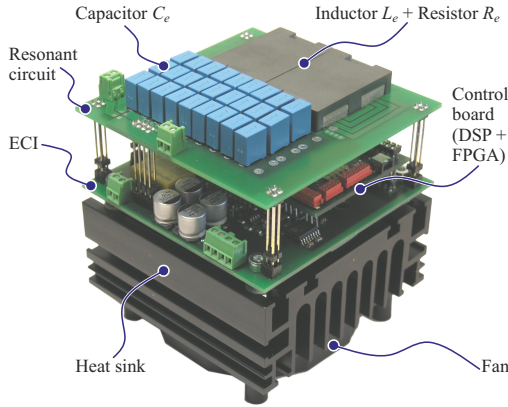


Fig. 10 Picture of the Electronically Controllable Impedance (ECI) hardware prototype with a series resonant circuit.

external magnetic field. The ECI, especially the power operational amplifier, is supplied by ± 12 V from a switched SW5250A source from Elgar. Since in the test setup the excitation voltage is not induced by an external field, the magnetic field \vec{H}_i generating air-coil [cf. Fig. 3(a)] was replaced by a PCB-inductor with a ferrite core (N87 with an air-gap). In this way, a more compact prototype could be built. The resistance R_e is thus mainly integrated in the inductor. The prototype's specifications are summarised in Table I. The power operational amplifier is directly mounted on the heat sink. In a next step, the linear amplifier could be replaced by a more efficient switched class D amplifier.

The measured path of the control algorithm (blue circles) in the $\Delta\phi_{ei}$ - z_{ei} -plane, which confirms the simulated one, is presented in Fig. 11. The time behaviour at the start (A) and end point (C) of the algorithm's path are shown in the figure as well.

Considering the measurements, two effects have to be shortly discussed. Firstly, the values of the inductor and resistor increase with temperature and thus with the current amplitude \hat{i}_e . For the waveforms at point (C), the estimated resistance is $R_e = 0.91 \Omega$ and the estimated inductance is $L_e = 394 \mu\text{H}$. Secondly, the amplitude of the excitation voltage u_e varies dependent on the total impedance \underline{Z}_{tot} . The more inductive the total impedance \underline{Z}_{tot} is, the more the

TABLE I Specifications of the prototype (the subscript *meas* indicates a measured quantity; for the simulations the calculated quantities were used).

Circuit	ETSRC	CCVS	Operational amplifier
R_e	0.8Ω	$\hat{i}_{out,max}$	10 A^*
$R_{e,meas}$	0.7Ω	$\hat{i}_{e,max}$	5 A
L_e	$360.0 \mu\text{H}$	$\hat{u}_{ei,max}$	30 V^*
$L_{e,meas}$	$366.2 \mu\text{H}$	$f_{out,max}$	100 kHz^*
C_e	$58.2 \mu\text{F}$		
$C_{e,meas}$	$58.4 \mu\text{F}$		
f_{self}	1.1 kHz		
$f_{self,meas}$	1.088 kHz		
Weight	815 g	Logic	DSP, FPGA
Length	96 mm	Excitation	Voltage u_e
Width	96 mm	Excitation waveform	Sine
Height	111 mm	\hat{u}_e	1.0 V
Volume	1 dm^3	f_e	1.0 kHz

*: Not simultaneously (thermal limitation)

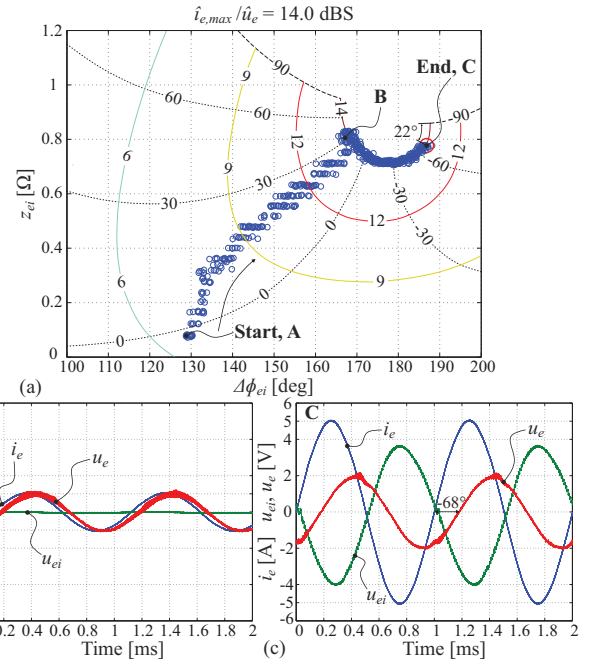


Fig. 11 Measured path of the control algorithm in the $\Delta\phi_{ei}$ - z_{ei} -plane (a), resonator current $i_e(t)$ (blue), ECI voltage $u_{ei}(t)$ (green) as well as excitation voltage $u_e(t)$ (red) at the start (b) and end point (c) for an emulated capacitive (paramagnetic) behaviour.

voltage amplitude drops and on the other side, the more capacitive the impedance is, the more the voltage is boosted. As a result, the voltage amplitude $\hat{u}_e(t)$, initially 1.0 V , first decreases to increase later on, and to reach 1.9 V at point C. Because the amplitude of the excitation voltage influences the trajectory of the equiquality-lines and of the phase ϕ_{tot} (of the total impedance \underline{Z}_{tot}) in the $\Delta\phi_{ei}$ - z_{ei} -plane, the equiquality-lines and ϕ_{tot} vary with time. This effect is more dominant than the one resulting from the temperature induced changes of the circuit components. In conclusion, the equiquality-lines and the phase ϕ_{tot} depicted in Fig. 11 are exemplary and combine the trajectories over time into one representative trajectory.

Despite the mentioned second point, the measurements confirm the simulations and the theoretical analysis to evoke a capacitive (paramagnetic) behaviour with a ETSRC. In addition, they prove that the ECI's control algorithm can cope with varying parameters.

The higher the frequency shift from f_{self} to f_e is, the greater the voltage u_{ei} becomes. Thus, in order not to exceed the maximal allowable voltage $\hat{u}_{ei,max} = 30 \text{ V}$, the maximum frequency shift is limited. With the values of the resistance and inductance given in Table I, the maximal self-resonant frequency f_{self} of the circuit in Fig. 3(b) is 1.91 kHz for an emulated paramagnetic and 1.88 kHz for a diamagnetic behaviour. The corresponding minimal frequency is 266 Hz for both cases.

V. FURTHER APPLICATIONS OF AN ECI

Further application area examples of the ECI concept are mainly in the domain of wireless energy transfer. These are:

- home electronic equipment such as mobile phones [14] or induction lamps [15],
- inductive charging of electric vehicles [16]–[19],

- power supply of biomedical equipment such as implants, stimulating and recording devices [20],
- inductive heating (printer-rolls [21], material surface processing [22]) as well as inductive cooking [23], [24].

VI. CONCLUSION

Magnetic stray fields of electric infrastructure for power distribution need to be shielded to reduce the required space, outside which the critical installation limit [rms-value of $B_e = 1 \mu\text{T}$ for the Swiss standard "Protection from Non-Ionising Radiation" (NISV)] is not exceeded. One approach could be to implement an active shield based on the concept of metamaterials. A metamaterial is in this case assembled by an array of base units, each one containing a LCR -resonator and a control unit called Electronically Controllable Impedance (ECI), where the inductor is formed by a conductive structure generating a magnetic field. An ECI consists of a 4-quadrant power converter with integrated measurement and control units for emulating an impedance in all four quadrants of the complex impedance plane. The current (or voltage) is measured and the voltage (or current) is outputted by the power converter according to an implemented control strategy.

The ECI and the LCR -resonator should allow the generation of a certain constant paramagnetic or diamagnetic behaviour of the metamaterial in a given region. Thus, the metamaterial could evoke an arbitrary constant resulting permeability μ_r' , which "guides" the magnetic field in space. The ECI adapts the resonant frequency of the resonators to the excitation frequency and adjusts the quality factor Q_{dB} . In addition, it allows the entire circuit, i.e. the electronically tuned series or parallel resonant circuit (ETSRC or ETPRC), to show a capacitive or inductive behaviour in order to emulate the paramagnetic or diamagnetic behaviour of the tuned metamaterial.

A control algorithm was designed and implemented in MATLAB/Simulink, which finds the operation points with the highest quality factor, under given voltage and current limitations. It further adjusts a capacitive or inductive behaviour of the circuit, regardless whether the circuit parameters are exactly known or not.

An ETSRC hardware prototype was built with a power operational amplifier as current controlled voltage source (CCVS) and the control algorithm was implemented on a DSP+FPGA to verify the proposed concept of the ECI. It is demonstrated that an actively controlled resonator exhibits a nearly five times higher current amplitude and that the resonant frequency of the resonant circuit could be shifted from 1.1 kHz to 1 kHz. The quality factor Q_{dB} could be increased by a factor of 22.2, from 0.6 dBS to 14.0 dBS. The experimental results confirm the simulations and thus the concept to emulate a capacitive (paramagnetic) behaviour with the ETSRC. Similarly, the concept could be verified for an ETPRC in a next step.

REFERENCES

- [1] J. Smajic, T. Steinmetz, B. Cranganu-Cretu, A. Nogues, R. Murillo, and J. Tepper, "Analysis of Near and Far Stray Magnetic Fields of Dry-Type Transformers: 3-D Simulations Versus Measurements," *IEEE Trans. Magn.*, vol. 47, no. 5, pp. 1374–1377, 2011.
- [2] T. Steinmetz and J. Smajic, *Magnetic stray field analysis of dry-type transformers – Simulation vs. measurement*. Presentation, ABB Switzerland Ltd., Corporate Research, 26 p., 2010.
- [3] *Verordnung über den Schutz vor nichtionisierender Strahlung (NISV)*. Swiss Confederation, Federal Office for the Environment, 22 p., 1999.
- [4] B. Hofmann, "Distribution Transformers and EMC," *Siemens, Special Reprint*, 8 p., 2009.
- [5] V. Veselago, L. Braginsky, V. Shklover, and C. Hafner, "Negative Refraction Index Materials," *Journal of Computational and Theoretical Nanoscience*, vol. 3, no. 2, pp. 1–30, 2006.
- [6] C. Caloz, "Perspectives on EM metamaterials," *Elsevier Ltd., Materialstoday*, vol. 12, no. 3, pp. 12–20, 2009.
- [7] P. Alitalo and S. Tretyakov, "Electromagnetic cloaking with metamaterials," *Elsevier Ltd., Materialstoday*, vol. 12, no. 3, pp. 22–29, 2009.
- [8] G. V. Eleftheriades and K. G. Balmain, Eds., *Negative-Refraction Metamaterials, Fundamental Principles and Applications*. IEEE Press, Wiley InterScience, 418 p., 2005.
- [9] J. B. Pendry, A. J. Holden, D. J. Robbins, and W. J. Stewart, "Magnetism from conductors and enhanced nonlinear phenomena," *IEEE Trans. Microw. Theory Tech.*, vol. 47, no. 11, pp. 2075–2084, 1999.
- [10] D. R. Smith, W. J. Padella, D. C. Vier, S. C. Nemat-Nasser, and S. Schultz, "Composite Medium with Simultaneously Negative Permeability and Permittivity," *Physical Review Letters*, vol. 84, no. 18, pp. 4184–4187, 2000.
- [11] M. Choi, S. H. Lee, Y. Kim, S. B. Kang, J. Shin, M. H. Kwak, K.-Y. Kang, Y.-H. Lee, N. Park, and B. Min, "A terahertz metamaterial with unnaturally high refractive index," *Nature Research Letter*, vol. 470, pp. 369–374, 2011.
- [12] A. Küchler, *Hochspannungstechnik, Grundlagen – Technologie – Anwendungen*, 2nd ed. Springer-Verlag Berlin Heidelberg, 543 p., 2005.
- [13] O. Sydoruk, O. Zhuromskyy, E. Shamonina, and L. Solymar, "Phonon-like dispersion curves of magnetoinductive waves," *Applied Physics Letters* 87, 3 p., 2005.
- [14] C.-G. Kim, D.-H. Seo, J.-S. You, J.-H. Park, and B. H. Cho, "Design of a contactless battery charger for cellular phone," *IEEE Trans. Ind. Electron.*, vol. 48, no. 6, pp. 1238–1247, 2001.
- [15] Philips, "Philips QL Induction Lighting Systems – Information for Original Equipment Manufacturers," 40 p., 2007.
- [16] M. L. G. Kissin, J. T. Boys, and G. A. Covic, "Interphase Mutual Inductance in Polyphase Inductive Power Transfer Systems," *IEEE Trans. Ind. Electron.*, vol. 56, no. 7, pp. 2393–2400, 2009.
- [17] N. A. Keeling, G. A. Covic, and J. T. Boys, "A Unity-Power-Factor IPT Pickup for High-Power Applications," *IEEE Trans. Ind. Electron.*, vol. 57, no. 2, pp. 744–751, 2010.
- [18] J. Sallan, J. L. Villa, A. Llombart, and J. F. Sanz, "Optimal Design of ICPT Systems Applied to Electric Vehicle Battery Charge," *IEEE Trans. Ind. Electron.*, vol. 56, no. 6, pp. 2140–2149, 2009.
- [19] U. K. Madawala and D. J. Thrimawithana, "A Bi-directional Inductive Power Interface for Electric Vehicles in V2G Systems," *IEEE Trans. Ind. Electron.*, no. 99, 2011, early access.
- [20] A. K. RamRakhyani, S. Mirabbasi, and M. Chiao, "Design and Optimization of Resonance-Based Efficient Wireless Power Delivery Systems for Biomedical Implants," *IEEE Trans. Biomed. Circuits Syst.*, vol. 5, no. 1, pp. 48–63, 2011.
- [21] H. Sugimura, H. Omori, S.-K. Kwon, H.-W. Lee, and M. Nakaoka, "High Efficiency Discrete Pulse Modulation Controlled High Frequency Series Load Resonant Soft Switching Inverter for Induction-Heated Fixing Roller," in *Proc. 37th IEEE Power Electronics Specialists Conf. PESC '06*, 2006, pp. 1–7.
- [22] Z. Wang, Z. Lou, and H. Chen, "A Novel Dual-LLC Resonant Soft Switching Converter for Super High Frequency Induction Heating Power Supplies," in *Proc. IEEE Power Electronics Specialists Conf. PESC 2007*, 2007, pp. 2561–2566.
- [23] O. Lucia, J. M. Burdio, I. Millan, J. Acero, and D. Puyal, "Load-Adaptive Control Algorithm of Half-Bridge Series Resonant Inverter for Domestic Induction Heating," *IEEE Trans. Ind. Electron.*, vol. 56, no. 8, pp. 3106–3116, 2009.
- [24] O. Lucia Gil, J. Burdio, L. Barragan, C. Carretero, and J. Acero, "Series Resonant Multi-Inverter with Discontinuous-Mode Control for Improved Light-Load Operation," *IEEE Trans. Ind. Electron.*, no. 99, 2011, early access.